

## RESULTS OF *GINGA*/*ROSAT* SIMULTANEOUS OBSERVATION OF THE X-RAY BURST SOURCE 1735–444

KWANG-IL SEON AND KYOUNG-WOOK MIN

Department of Physics, Korea Advanced Institute of Science and Technology, 373-1 Gusong-dong, Yusong-gu, Taejon 305-701, Korea;  
kiseon@space.kaist.ac.kr, kwmin@space.kaist.ac.kr

KENJI YOSHIDA

Kanagawa University, 3-27-1, Rokkakubashi, Kanagawa-ku, Yokohama 221, Japan; yoshida@xray.astro.isas.ac.jp

FUMIYOSHI MAKINO

Institute of Space and Astronautical Science, 3-1-1, Yoshinodai, Sagami-hara, Kanagawa 229, Japan; makino@xray.astro.isas.ac.jp

WALTER H. G. LEWIN

Massachusetts Institute of Technology, Center for Space Research, Room 37-627, Cambridge, MA 02139, USA; lewin@space.mit.edu

AND

MICHIEL VAN DER KLIS AND JAN VAN PARADIJS

Astronomical Institute “Anton Pannekoek,” University of Amsterdam; and Center for High-Energy Astrophysics,  
Kruislaan 403, NL-1098 SJ Amsterdam, Netherlands; michiel@astro.uva.nl, jvp@astro.uva.nl

Received 1996 April 17; accepted 1996 October 28

### ABSTRACT

We present a detailed analysis of simultaneous *Ginga* and *ROSAT* observations of the X-ray burst source 1735–444, during which the source was in an unusually high luminosity state. The source shows the characteristics of an atoll source in the high-intensity (banana) state, with a general correlation between intensity and spectral hardness. A blackbody component contributes  $\sim 15\%$ – $20\%$  of the total flux when the conventional two-component model is used to fit the spectra. We also observed a bright burst with radius expansion at this very high luminosity. The burst spectrum could not be described by a simple blackbody model. We discuss possible explanations.

*Subject headings:* binaries: close — stars: individual (1735–444) — X-rays: bursts — X-rays: stars

### 1. INTRODUCTION

The low-mass X-ray binaries (LMXBs) are generally believed to be weakly magnetized neutron stars accreting material from a late-type companion star by Roche lobe overflow. LMXBs can be classified into two classes: faint X-ray bursters and bright nonbursting sources, according to their luminosity. The burst sources have persistent X-ray luminosities on the average less than a few tenths of the Eddington limit, while the luminosities of the nonbursting sources are higher than this value.

Another classification is possible, according to Hasinger & van der Klis (1989), in which LMXBs are divided into Z and atoll sources based on their rapid X-ray variability and spectral properties. Type I X-ray bursts from LMXBs show a great variety in their properties, not only from source to source but also in different bursts seen from an individual source. Global properties of type I bursts are well described qualitatively by the thermonuclear flash in the surface layers of accreting neutron stars (see Lewin, van Paradijs, & Taam 1993 for a recent review).

The X-ray burst source 1735–444 was the first burst source to be optically identified (McClintock et al. 1977); its optical counterpart is a faint ( $V = 17$ ) blue emission-line star, V926 Sco. The source was discovered as a burst source in 1977 by Lewin et al. (1977). This is also the first burst source from which X-ray and optical bursts were observed simultaneously (Grindlay et al. 1978). The first accurate determination of the orbital period of 1735–444 was presented by Corbet et al. (1986). They derived a period of  $4.654 \pm 0.005$  hr from an analysis of the optical observation. The period was confirmed by van Amerongen, Pedersen, & van Paradijs (1987). Simultaneous X-ray and

optical observations of 1735–444 have been performed by several authors (Smale et al. 1986; Corbet et al. 1989), and their results confirmed that the major contribution to the optical (burst and persistent) emission comes from X-ray heating of the accretion disk formed around a neutron star (see van Paradijs & McClintock 1995 for a general review). Possible optical flares, which are somewhat reminiscent of the type II bursts seen in the Rapid Burster, have been reported by Imamura, Steiman-Cameron, & Middleditch (1987) and Beskin et al. (1994).

The source 1735–444 is one of the brightest persistent X-ray sources among the burst sources, but is relatively faint in comparison with Z sources (van Paradijs, Penninx, & Lewin 1988a). Hasinger & van der Klis (1989) classified 1735–444 as an atoll source that shows two spectral states characterized by the “island” and “banana” branches in an X-ray color-color diagram. The bursting and persistent X-ray behavior of 1735–444 have been studied extensively with *SAS 3* (Lewin et al. 1980) and with *EXOSAT* (van Paradijs et al. 1988b). These observations showed that the burst intervals are highly irregular, ranging from  $\sim 30$  minutes to more than 50 hr, without an obvious correlation with the persistent X-ray flux that fuels the bursts. Penninx et al. (1989) investigated the presence of quasi-periodic oscillation and low-frequency noise (LFN) but found none. An iron line at 6.8 keV with equivalent width  $\sim 90$  eV was detected with *EXOSAT* (Smale et al. 1986), but a 90% confidence upper limit of 23 eV was obtained with *Tenma* (Hirano et al. 1987).

Two-component spectral models of various types, usually a blackbody component together with some other component, e.g., a multicolor disk blackbody, thermal brems-

strahlung, or a power law with an exponential cutoff, have been suggested as descriptions of the observed spectrum of several bright LMXBs (Serlemitsos & Swank 1980; Mitsuda et al. 1984; White, Peacock, & Taylor 1985). Many authors believe these two components are associated with two physical sites of X-ray emission, generally taken to be the neutron star surface and the inner accretion disk or the accretion disk corona (Mitsuda et al. 1984; White, Stella, & Parmar 1988). Spectral analyses of the persistent emission of 1735–444 have been performed using a power law with an exponential cutoff or a thermal bremsstrahlung model (Smale et al. 1986; van Paradijs et al. 1988b; Penninx et al. 1989).

In this paper we report the results of an analysis of simultaneous *Ginga* and *ROSAT* observations of 1735–444. During the observations, the persistent X-ray emission was the strongest ever observed, and an unusually bright X-ray burst was detected. The X-ray observations and the light curves are summarized in § 2. The detailed spectral analysis of the persistent emission is presented in § 3; the burst is discussed in § 4. Possible physical interpretations are given in § 5.

## 2. OBSERVATION AND LIGHT CURVES

The source 1735–444 was observed with the large-area proportional counters (LACs; Makino et al. 1987; Turner et al. 1989) on board *Ginga* between 1991 September 27, 9:59 UT, and September 28, 22:40 UT, and between September 29, 13:10 UT, and September 29, 15:10 UT. Simultaneous observations were made with the position sensitive proportional counters (PSPCs; Pfeffermann et al. 1987) on board the Röntgen satellite (*ROSAT*; Trümper 1983) between September 27, 9:21 UT, and September 28, 8:56 UT. The LAC consists of eight identical proportional counters with a total effective area of 4000 cm<sup>2</sup>. It covers an energy range from 1 to 37 keV with 48 channels in the data modes MPC1 and MPC2 and has an energy resolution of 18% at 6 keV. The LAC observation of the source was performed in the telemetry mode MPC2 in the nominal gain mode. The PSPC covers an energy range from 0.1 to 2.4 keV and has an energy resolution of 45% at 0.93 keV.

The observations were interrupted due to Earth occultations and passage through the South Atlantic Anomaly and other high-energy particle background episodes. The background subtraction for the analysis of the *Ginga* observations was done using the nearby sky data obtained 2 days after the observation. Background spectra for the *ROSAT* observations were obtained from nearby skies around the source in the field of view of the PSPC.

The *ROSAT* light curve is shown in Figure 1a. The total count rate in the energy band 0.1–2.4 keV varies from ~50 to ~100 counts s<sup>-1</sup>. The light curve (1–37 keV) and the spectral hardness ratios of the *Ginga* observations are plotted in Figures 1b–1d. The hard color ratio is calculated as the count rate ratio of the 6.4–19.8 keV band to the 4.7–6.4 keV band, and the soft color ratio as the ratio of the 2.9–4.7 keV band to the 1.7–2.9 keV band. Each point in Figure 1 represents the data averaged over 240 s. We observed one burst at 1991 September 28, 21:17:15 UT, as indicated by the vertical line in Figure 1b. The total *Ginga* count rate varies from ~2000 to ~3400 counts s<sup>-1</sup> except during the burst, when the count rate went up to ~8200 counts s<sup>-1</sup>. The total count rate during the short *Ginga* observation on September 29 was ~2200 counts s<sup>-1</sup> (not

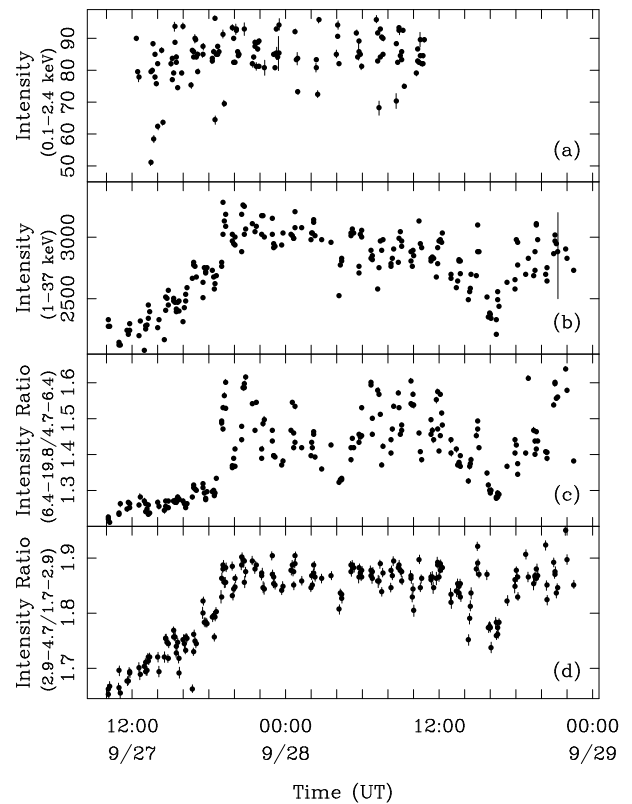


FIG. 1.—(a) Light curve of *ROSAT* observation in 0.1–2.4 keV. (b) X-ray light curve in 1–37 keV. (c) The hard hardness ratio, a ratio of the 6.4–19.8 to the 4.7–6.4 keV flux. (d) The soft hardness ratio, a ratio of the 2.9–4.7 to the 1.7–2.9 keV flux. Each data point is an accumulation for 240 s after background subtraction and aspect correction. The intensity is given in counts per second.

shown in the figure). During the initial stage the total count rate increased slowly by 50% in ~12 hr. Then the count rate remained at this high level except around September 28 at 16:30 UT. The luminosities varied between ~0.84 and  $1.32 \times 10^{38} (d/10 \text{ kpc})^2 \text{ ergs s}^{-1}$ , the highest levels observed so far for this source. From Figures 1b–1d it can be seen that the count rate changes are clearly correlated with the variations in the hardness ratios, and that the hard ratio shows larger fluctuations than the soft ratio.

## 3. PERSISTENT EMISSION

### 3.1. Color-Color Diagram and Timing Analysis

We plot color-color and intensity-color diagrams in Figure 2. Each data point in Figure 2 represents an accumulation in 150 s. The intensity is given in counts per second. The color-color diagram shows only one branch in the present observation. During the first stage of the observation the source occupies the lower part in the color-color and the intensity-color diagrams, and then moves to the upper part. The branch we observed can be identified as the “banana” branch of an atoll source (Hasinger & van der Klis 1989). The spectral state of the data on September 29 occupied again the lower parts (marked with open circles in Fig. 2). The state just prior to the burst is marked by a triangle. The spectral parameters of the burst itself are outside the range of Figure 2; the soft color, hard color, and intensity of the burst are  $2.22 \pm 0.03$ ,  $1.52 \pm 0.02$ , and  $5065 \pm 49$ , respectively.

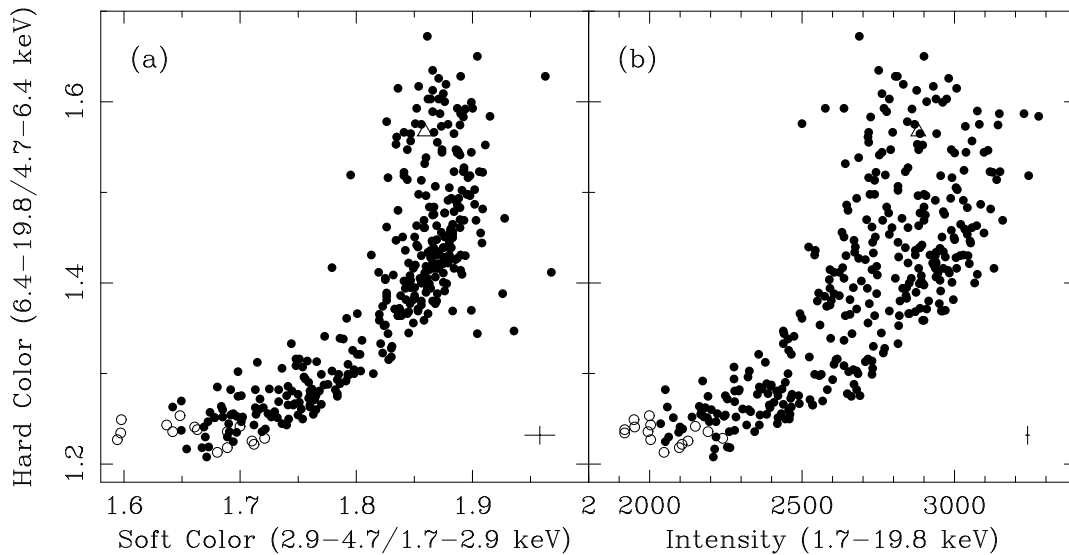


FIG. 2.—(a) Color-color diagram and (b) hardness-intensity diagram. Each data point is an accumulation for 150 s. The intensity is given in counts per second. The cross at the lower right-hand corner denotes a typical error bar. A state just prior to the burst is indicated by a triangle. The spectral states of the data on September 28 and on September 29 are marked with closed circles and open circles, respectively.

Because of the lack of high time resolution, a detailed analysis of power spectra could not be performed. The power spectrum in Figure 3a, obtained using the data of the highest time resolution 0.0625 s at the lower banana state, shows a power-law red noise component with a slope ( $\alpha$ ) of  $-1.33 \pm 0.20$ , which can be identified as the very low frequency noise (VLFN), and a flat component above  $\sim 1$  Hz (Hasinger & van der Klis 1989). The fractional rms variation integrated over 0.005–1 Hz is  $1.91\% \pm 0.70\%$ . The strength of the power spectra of the VLFN increases, as the source moves from the lower part of the banana to the upper part (Fig. 3b). The best-fit value of  $\alpha$  and the fractional rms variation for the upper part of the banana are  $-1.31 \pm 0.03$  and  $2.63\% \pm 0.16\%$ , respectively. However, we were able to obtain a power spectrum only up to 1 Hz for the upper banana branch because of the lack of high time resolution data. Nevertheless, the present result shows

characteristics of the power spectra similar to those of other atoll sources in the banana state.

### 3.2. Spectral Analysis

We have investigated the *Ginga* spectral data of 1735–444 using simple spectral models. Observations made with *Einstein*, using higher spectral resolution than that available to us, have shown that in the 1 keV range the X-ray spectrum of this source contains a large number of emission lines (Vrtilek et al. 1991). This shows that simple spectral models, as employed by us, can only be considered as approximations. We analyzed the persistent X-ray spectrum of 1735–444 using the data averaged over the whole observation period including the data set of September 29. As can be seen from Table 1, no simple single-component models can adequately describe the spectrum. We have also tried several well-known two-component models to fit the

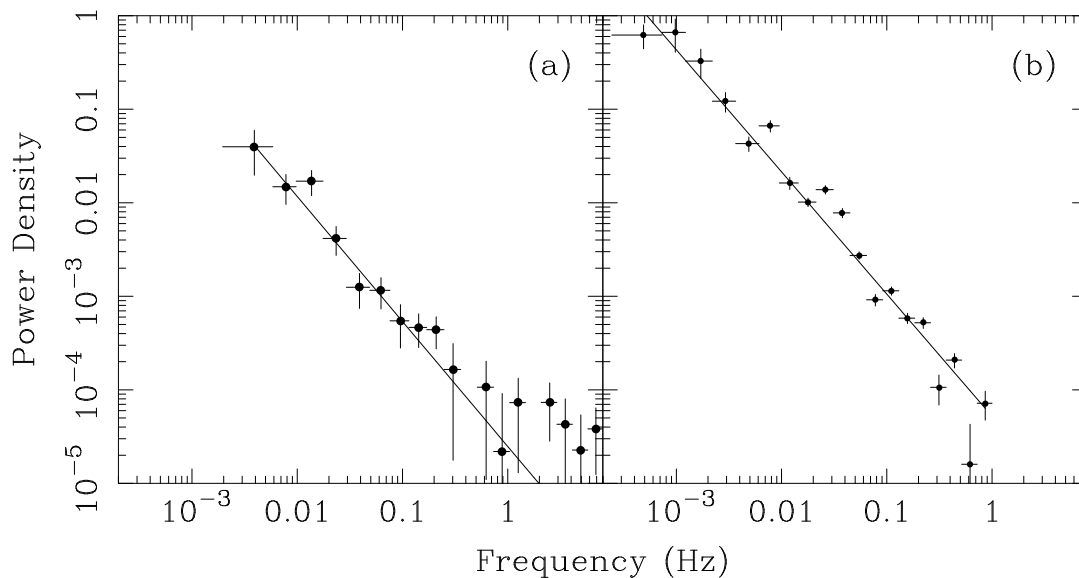


FIG. 3.—Power spectra obtained (a) for the lower banana state and (b) for the upper banana state

TABLE 1  
REDUCED  $\chi^2$  VALUES FOR SEVERAL MODELS

Model	$\chi^2_v(\text{dof})$
BREMSS <sup>a</sup> .....	70.0(34)
PL <sup>b</sup> .....	437(34)
PLEC <sup>c</sup> .....	12.9(32)
COMPST <sup>d</sup> .....	6.38(33)
DISKBB <sup>e</sup> .....	31.8(34)
BREMSS + BBODY .....	2.16(32)
DISKBB + BBODY .....	4.09(32)
DISKBB + CMPB <sup>f</sup> .....	1.61(31)
DISKBB + CMPB + REFLW <sup>g</sup> .....	1.03(30)
PLEC + BBODY .....	0.43(30)
COMPST + BBODY .....	0.85(31)
COMPST + BBODY + GAUSS <sup>h</sup> .....	0.49(29)

<sup>a</sup> Thermal bremsstrahlung.

<sup>b</sup> Power law.

<sup>c</sup> Power law with exponential cutoff.

<sup>d</sup> Comptonization model (Sunyaev & Titarchuk 1980).

<sup>e</sup> Disk blackbody.

<sup>f</sup> Comptonized blackbody.

<sup>g</sup> Reflection model (Lightman & White 1988).

<sup>h</sup> Gaussian line.

observed spectrum, and the following models gave reasonable  $\chi^2_v$  values: (1) a combination of a multicolor disk blackbody and a Comptonized blackbody (DISKBB + CMPB), (2) a power law with an exponential cutoff and a blackbody (PLEC + BBODY), and (3) a Comptonization model (Sunyaev & Titarchuk 1980) and a blackbody (COMPST + BBODY). However, we found several local minima for PLEC + BBODY and DISKBB + CMPB. The blackbody temperature,  $\sim 2.5$  keV, obtained from PLEC + BBODY seems rather high. The residuals in DISKBB + CMPB show a wavy feature with a broad excess around 7 keV and an absorption-like structure in the energy range from 8 to 12 keV. Hence, we adopt COMPST + BBODY for the continuum model in the present study. The fitting improves when a Gaussian line at 6.79 keV with equivalent width  $51^{+22.2}_{-22.0}$  eV is included. The obtained line-center energy is consistent with the previous result (Smale et al. 1986) and those from the spectra of other LMXBs (White et al. 1986). The iron line in the present analysis seems to be of the recombination origin.

Recently, Mitsuda (1992) and Yoshida et al. (1993) adopted the reflection model to explain the broad excess and the absorption feature, which occurs when one tries to

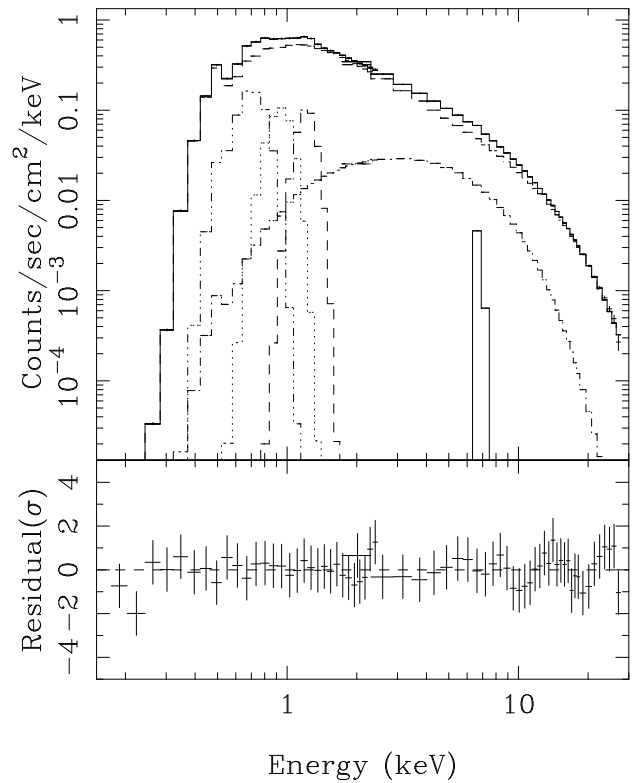


FIG. 4.—Unfolded energy spectra and the best-fit model for the simultaneous *Ginga* and *ROSAT* observations. The continuum model is COMPST + BBODY.

fit the *Ginga* data of some LMXBs. The reflection model was originally suggested for the spectra of active galactic nuclei (Lightman & White 1988; Guilbert & Rees 1988) and Galactic black hole candidates (Ebisawa et al. 1992; Done et al. 1992). We used the reflection model calculated by Lightman & White (1988) to fit the observed spectra, although the model is valid for a power-law shape incident photon spectrum and has only three parameters to represent the ionization state of plasma reflecting the incident photons, i.e.,  $\xi = 0.0, 0.02, \text{ and } 2.0$ . Among the three ionization parameters, the model with  $\xi = 0.02$  gives the best fit, with the reduced  $\chi^2$  value  $\sim 1.0$  for 30 dof. However, the best-fit parameters are unrealistic. The temperature at the inner disk radius was 3.15 keV, which is too high, while the blackbody temperature  $T_b$ , 0.12 keV, is too low, as it trans-

TABLE 2

A. BEST-FIT PARAMETERS FOR THE PERSISTENT SPECTRA

COMPST			BBODY				$\chi^2_v(\text{dof})$
$F_{\text{COMPST}}^a$	$kT_e^b$	$\tau$	$F_b^a$	$kT_b^b$	$R_b^c$	$N_H^d$	
$8.15^{+0.29}_{-0.28}$	$3.14^{+0.09}_{-0.08}$	$13.11^{+0.50}_{-0.52}$	$1.40^{+0.18}_{-0.16}$	$1.69^{+0.08}_{-0.09}$	$4.02^{+0.25}_{-0.23}$	$3.50^{+0.17}_{-0.16}$	0.45(55)

B. LINES							
$E_{\text{line}}^e$	EW <sup>f</sup>	$E_{\text{line}}$	EW	$E_{\text{line}}$	EW	$E_{\text{line}}$	EW
0.65(fixed)	$119^{+50.0}_{-40.5}$	0.92(fixed)	$52.4^{+18.3}_{-26.0}$	$1.21^{+0.08}_{-0.09}$	$51.2^{+26.5}_{-17.7}$	$6.79^{+0.31}_{-0.30}$	$51.0^{+22.2}_{-22.0}$

NOTE.—Quoted errors are 90% confidence limits.

<sup>a</sup> In units of  $10^{-9}$  ergs  $\text{cm}^{-2} \text{s}^{-1}$ .

<sup>b</sup> Electron temperature and blackbody temperature are given in units of keV.

<sup>c</sup> Blackbody radius is given in units of km.

<sup>d</sup> In units of  $10^{21} \text{ cm}^{-2}$ .

<sup>e</sup> Line energies are given in units of keV.

<sup>f</sup> Equivalent width is given in units of eV.

TABLE 3  
FLUX AND BEST-FIT PARAMETERS FOR THE TIME-SLICED ENERGY SPECTRA

NUMBER	START	END	COMPTONIZATION MODEL			BLACKBODY			LINE EW (eV)	$\chi^2_d$
			$F_{\text{COMPST}}^a$	$kT_e^b$ (keV)	$\tau$	$F_b^c$	$kT_b$ (keV)	$R_b$ (km)		
1	27 09:58	27 13:31	$6.79^{+0.26}_{-0.25}$	$3.11^{+0.10}_{-0.08}$	$12.01^{+0.42}_{-0.47}$	$0.89^{+0.19}_{-0.14}$	$1.45^{+0.09}_{-0.10}$	$4.34^{+0.44}_{-0.36}$	$59.9^{+23.2}_{-23.1}$	0.66
2	27 13:39	27 16:21	$6.93^{+0.27}_{-0.26}$	$3.17^{+0.11}_{-0.10}$	$11.93^{+0.47}_{-0.49}$	$1.33^{+0.17}_{-0.15}$	$1.54^{+0.07}_{-0.07}$	$4.70^{+0.30}_{-0.27}$	$58.5^{+22.6}_{-22.6}$	0.56
3	27 16:41	27 17:54	$7.83^{+0.32}_{-0.31}$	$3.08^{+0.12}_{-0.10}$	$12.57^{+0.56}_{-0.61}$	$1.40^{+0.20}_{-0.17}$	$1.59^{+0.08}_{-0.09}$	$4.51^{+0.31}_{-0.28}$	$65.6^{+22.9}_{-23.1}$	1.09
4	27 18:15	27 21:28	$8.80^{+0.36}_{-0.33}$	$3.15^{+0.12}_{-0.10}$	$13.44^{+0.64}_{-0.71}$	$1.54^{+0.21}_{-0.20}$	$1.76^{+0.10}_{-0.12}$	$3.87^{+0.25}_{-0.26}$	$54.0^{+22.3}_{-22.2}$	0.38
5	27 21:31	28 03:39	$8.76^{+0.37}_{-0.34}$	$3.14^{+0.12}_{-0.10}$	$13.44^{+0.66}_{-0.72}$	$1.76^{+0.21}_{-0.20}$	$1.77^{+0.09}_{-0.10}$	$4.08^{+0.24}_{-0.24}$	$55.5^{+22.0}_{-22.1}$	0.51
6	28 03:45	28 06:02	$8.52^{+0.36}_{-0.33}$	$3.15^{+0.13}_{-0.10}$	$13.29^{+0.65}_{-0.70}$	$1.67^{+0.21}_{-0.19}$	$1.71^{+0.09}_{-0.10}$	$4.28^{+0.26}_{-0.25}$	$44.6^{+22.4}_{-22.3}$	0.77
7	28 06:36	28 10:06	$8.51^{+0.38}_{-0.34}$	$3.26^{+0.15}_{-0.13}$	$13.16^{+0.80}_{-0.82}$	$1.73^{+0.23}_{-0.25}$	$1.90^{+0.09}_{-0.12}$	$3.51^{+0.23}_{-0.26}$	$47.7^{+22.1}_{-22.1}$	0.51
8	28 10:14	28 10:41	$8.92^{+0.40}_{-0.37}$	$3.06^{+0.14}_{-0.11}$	$13.87^{+0.76}_{-0.86}$	$1.46^{+0.24}_{-0.22}$	$1.68^{+0.11}_{-0.15}$	$4.15^{+0.33}_{-0.32}$	$55.6^{+23.5}_{-23.4}$	0.74
9	28 10:14	28 12:21	$8.72^{+0.38}_{-0.34}$	$3.14^{+0.14}_{-0.11}$	$13.67^{+0.74}_{-0.81}$	$1.54^{+0.21}_{-0.22}$	$1.79^{+0.10}_{-0.13}$	$3.73^{+0.25}_{-0.28}$	$51.9^{+22.4}_{-22.3}$	0.55
10	28 12:29	29 15:12	$7.68^{+0.34}_{-0.32}$	$3.23^{+0.15}_{-0.13}$	$12.70^{+0.73}_{-0.75}$	$1.82^{+0.19}_{-0.20}$	$1.78^{+0.07}_{-0.09}$	$4.14^{+0.21}_{-0.23}$	$54.6^{+22.4}_{-22.4}$	0.67
11	28 15:41	28 17:15	$6.99^{+0.29}_{-0.28}$	$3.09^{+0.12}_{-0.10}$	$12.74^{+0.57}_{-0.62}$	$1.32^{+0.19}_{-0.16}$	$1.55^{+0.08}_{-0.09}$	$4.62^{+0.32}_{-0.28}$	$58.4^{+23.2}_{-23.2}$	0.62
12	28 17:19	28 22:34	$8.50^{+0.35}_{-0.32}$	$3.05^{+0.11}_{-0.09}$	$13.99^{+0.63}_{-0.72}$	$1.36^{+0.21}_{-0.19}$	$1.71^{+0.11}_{-0.13}$	$3.88^{+0.29}_{-0.28}$	$55.0^{+22.4}_{-22.2}$	0.39

NOTE.—Quoted errors are 90% confidence limits. Center energy of Gaussian line is fixed at 6.79 keV.

<sup>a</sup> Flux of Comptonization model in units of  $10^{-9}$  ergs  $\text{cm}^{-2}$   $\text{s}^{-1}$ .

<sup>b</sup> Electron temperature.

<sup>c</sup> Flux of the blackbody in units of  $10^{-9}$  ergs  $\text{cm}^{-2}$   $\text{s}^{-1}$ .

<sup>d</sup> dof = 28.

lates into too large a blackbody radius to be interpreted as emission from the neutron star surface.

Since the combination of COMPST and BBODY gave a reasonable fit to the *Ginga* data, we tried to fit the *ROSAT* and *Ginga* data simultaneously with this model. In the spectral fit, we used the same time filters for the data of both satellites, which comprises about 70% of the *Ginga* data and

about 76% of the *ROSAT* data. But there remained a broad excess in the energy range from 0.6 to 1.4 keV. We found from many attempts that the inclusion of two Gaussian lines representing the eight emission lines detected by Vrtilik et al. (1991) improves the fit. We thus added the two Gaussian lines, in which the line energies were held constant at 0.92 and 0.65 keV, as in Table 2. These center energies correspond to the emission lines from the Fe xvii and Fe xviii and the O viii ions, respectively. The equivalent widths of the 0.92 and 0.65 keV lines are  $52^{+18.3}_{-26.0}$  and  $119^{+50.0}_{-40.5}$  eV, respectively. The line widths were assumed to be negligible. We still find an excess around  $\sim 1.2$  keV, although the reduced  $\chi^2 \sim 1.0$  for 57 dof is good. The inclusion of a Gaussian line with a center energy of  $\sim 1.2$  keV improved the goodness of the fit. The emission line at  $E \sim 1.2$  keV was observed in spectra of several sources, but not for 1735–444 (Vrtilik et al. 1991). The reduced  $\chi^2$  is 0.45 for 55 dof after the inclusion of the line. The unfolded spectrum and the model are shown in Figure 4. The inclusion of the lines at low energy might underline the need for careful interpretations of the fit parameters that come out of the spectral fits made of the rather low resolution data.

We divided the *Ginga* data into 12 intensity bins to investigate the change of fitting parameters according to the intensity level. We used COMPST + BBODY for the two-component model. Table 3 shows the observation time and the best-fit spectral parameters. The blackbody component contributes from 15% to 28% to the total flux. Figure 5 shows the best-fit parameters plotted against the total flux. Both components COMPST and BBODY tend to increase with the total flux. The electron temperature  $kT_e$  does not show a clear correlation with the total flux. The scattering depth  $\tau$  and the blackbody temperature  $kT_b$  show positive correlation with the total flux, which reflects the correlation between the intensity level and the hardness ratios described in § 3.1.

The apparent blackbody radius, calculated under the assumption that the observed flux during the persistent emission is from a spherically symmetric body, is  $\sim 4$  km. It is interesting to note that 1820–303, which is another lumi-

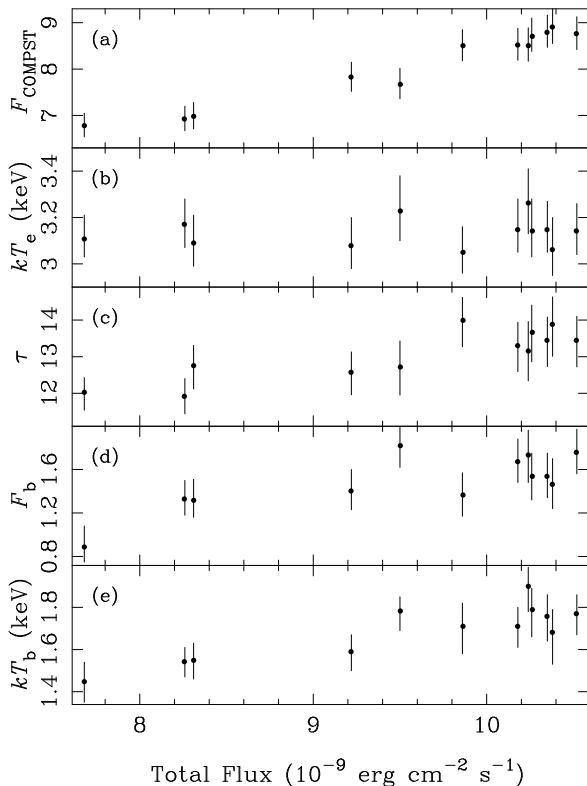


FIG. 5.—Best-fit parameters of COMPST + BBODY model for 12 data sets plotted against the total flux: (a) flux of the COMPST component; (b) electron temperature  $kT_e$ ; (c) scattering depth  $\tau$ ; (d) flux of the BBODY component; and (e) blackbody temperature  $kT_b$ . The fluxes are given in units of  $10^{-9}$   $\text{cm}^{-2}$   $\text{s}^{-1}$ .

nous X-ray burster, shows also a small blackbody radius in the persistent spectrum (Haberl et al. 1987).

#### 4. BURST

The light curves of the burst are shown in Figure 6. The observation was performed in the low bit rate MPC2 telemetry mode with a time resolution of 2 s. The energy-dependent burst profile is evident in the spectral bands plotted in the figure, in spite of the limited time resolution. The profiles are characteristic of radius expansion and subsequent contraction of the photosphere of the neutron star at approximately constant bolometric Eddington luminosity (for a review see Lewin et al. 1993).

The time-resolved spectra were obtained in 2 s intervals through the peak of the burst, and in 6 s intervals during the decay stages, A, B, C, D, E, and F, as indicated in Figure 6. We subtracted the persistent spectrum plus background accumulated over  $\sim 600$  s just prior to the burst and fitted the net burst spectra using a conventional blackbody model, as many authors have done previously. However, the uncertainties in the  $N_H$  values are very large because of the limited statistics in individual bins. A lower column density does improve the fit marginally, but it is not well constrained by the data. We therefore adopted a fixed value for  $N_H$  of  $3.5 \times 10^{21} \text{ cm}^{-2}$ , which was derived from the spectrum of the persistent emission. The best-fit parameters are shown in Table 4. A simple blackbody model gives a rather poor fit for spectra C–E. The time variation of the bolometric flux, the blackbody temperature, and the apparent radius of the emission region, assuming isotropic radiation, are shown in Figure 7. Because of the photospheric expansion, the blackbody temperature decreases at the peak luminosity while the radius increases. The bolometric peak flux  $F_{\text{max}}$  is  $\sim 1.5 \times 10^{-8} \text{ ergs cm}^{-2} \text{ s}^{-1}$ , corresponding to the luminosity  $L_{\text{max}} \simeq 1.8 \times 10^{38} \text{ ergs s}^{-1}$ , assuming a distance of 10 kpc. However, since the peak flux was smeared out because of the coarse time resolution, the real peak flux may have been larger than this. The color temperature decreases to  $\sim 1.4$  keV in the tail of the burst. The

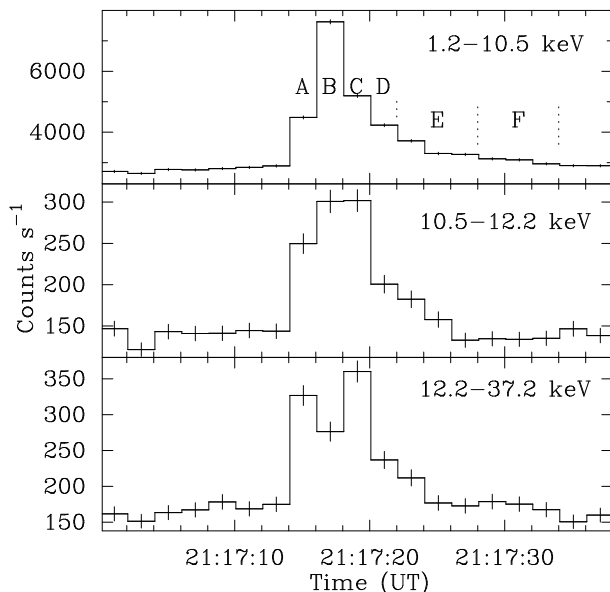


FIG. 6.—Light curves in three energy bands (1.2–10.5, 10.5–12.2, and 12.2–37.2 keV) of the burst are shown. A–E represent the time intervals for which separate spectral analyses are carried out.

TABLE 4  
BEST-FIT BLACKBODY PARAMETERS (BURST)

Data	$F_b^a$	$kT_b^b$	$R_b^c$	$\chi^2(\text{dof})$
A .....	$7.86_{-0.39}^{+0.38}$	$2.33_{-0.09}^{+0.08}$	$5.01_{-0.33}^{+0.31}$	0.93(32)
B .....	$15.57_{-0.38}^{+0.38}$	$1.66_{-0.03}^{+0.03}$	$13.77_{-0.49}^{+0.48}$	0.86(32)
C .....	$10.06_{-0.40}^{+0.39}$	$2.15_{-0.07}^{+0.06}$	$6.63_{-0.37}^{+0.35}$	2.08(32)
D .....	$5.10_{-0.29}^{+0.29}$	$1.76_{-0.09}^{+0.08}$	$7.05_{-0.64}^{+0.60}$	1.76(32)
E .....	$2.29_{-0.14}^{+0.14}$	$1.56_{-0.08}^{+0.09}$	$6.01_{-0.62}^{+0.57}$	2.06(32)
F .....	$1.10_{-0.12}^{+0.12}$	$1.40_{-0.16}^{+0.14}$	$5.18_{-1.11}^{+0.93}$	1.10(32)

NOTE.—Quoted errors are 90% confidence limits.

<sup>a</sup> Bolometric flux of blackbody in units of  $10^{-9} \text{ ergs cm}^{-2} \text{ s}^{-1}$ .

<sup>b</sup> Blackbody temperature in units of keV

<sup>c</sup> Blackbody radius, for an assumed distance 10 kpc, in units of km.

apparent radius in the tail is  $\sim 5.4$  km, which is larger than the value during the persistent emission. The burst fluence is  $E_b = 9.6 \times 10^{-8} \text{ ergs cm}^{-2}$ .

In addition to the systematic wavy nature in the residuals, the simple blackbody model yields high-energy excess above  $\sim 10$  keV, especially during the decay of the burst. Such excess has previously been found in burst spectra from 1608–522 (Nakamura et al. 1989). Nakamura et al. argued that these high-energy excesses are caused by the inverse Compton scattering of blackbody photons. We therefore tried a Comptonized blackbody model to fit the burst spectra during the decay. The fit to spectrum C is still not good enough, although the model generally improves the fit, as shown in Table 5. However, 1735–444 had a high luminosity when the present burst with high-energy excess was observed, while the high-energy excess in the 1608–522 spectra might be related to its low luminosity at the time of observation, as suggested by Nakamura et al. (1989).

More recently, Day & Done (1991) suggested that disk reflection can furnish the hard photons seen by Nakamura et al. (1989). They argue that a disk-reflected component is best seen just after the burst peak, when the reflected

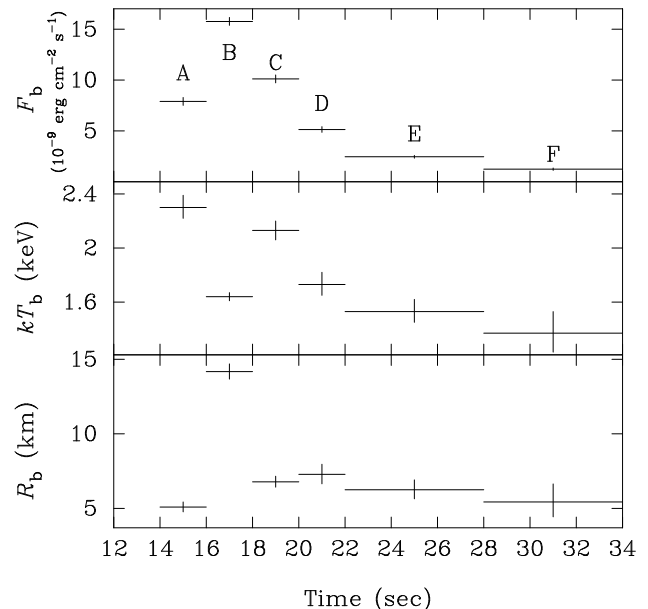


FIG. 7.—Time variation of the bolometric flux, the blackbody temperature, and the apparent blackbody radius. A spherical blackbody radiation is assumed in this calculation.

TABLE 5  
BEST-FIT COMPTONIZED BLACKBODY PARAMETERS (BURST)

Data	$F_{\text{compb}}^a$	$kT_b^b$	$y^c$	$\chi^2(\text{dof})$
C .....	$11.35^{+1.63}_{-1.76}$	$1.99^{+0.09}_{-0.10}$	$0.26^{+0.11}_{-0.12}$	1.79(31)
D .....	$3.97^{+0.65}_{-0.70}$	$1.62^{+0.09}_{-0.09}$	$0.24^{+0.13}_{-0.13}$	1.56(31)
E .....	$1.87^{+0.30}_{-0.32}$	$1.36^{+0.10}_{-0.11}$	$0.37^{+0.13}_{-0.13}$	1.52(31)
F .....	$0.93^{+0.24}_{-0.28}$	$1.15^{+0.16}_{-0.18}$	$0.48^{+0.22}_{-0.21}$	0.77(31)

NOTE.—Quoted errors are 90% confidence limits.

<sup>a</sup> Flux of Comptonized blackbody in units of  $10^{-9}$  ergs  $\text{cm}^{-2}$   $\text{s}^{-1}$ .

<sup>b</sup> Blackbody temperature in units of keV.

<sup>c</sup> Comptonization parameter.

photons, delayed by their passage to the site of reflection, appear in stronger contrast to the fast-declining primary emission from the cooling neutron star. The burst spectra were therefore fitted using a model that combines a blackbody with a lower temperature and a reflected blackbody component with a higher temperature. The reflection model based on the work of Lightman & White (1988) was used. The best-fit parameters are shown in Table 6. The uncertainty ranges of the fit parameters are too large to determine the parameters accurately. Although disk reflection can account for the high-energy excess, the wavy nature in the residuals still remains in the present case. Also, the residuals show no evidence of the absorption edge that is expected from the disk reflection (Day & Done 1991).

Van Paradijs & Lewin (1985) pointed out that spectral analyses of X-ray bursts are systematically affected if the persistent emission contains a spectral component that originates from the outer layer of a hot neutron star. The “standard” analysis of X-ray burst spectra, in which a

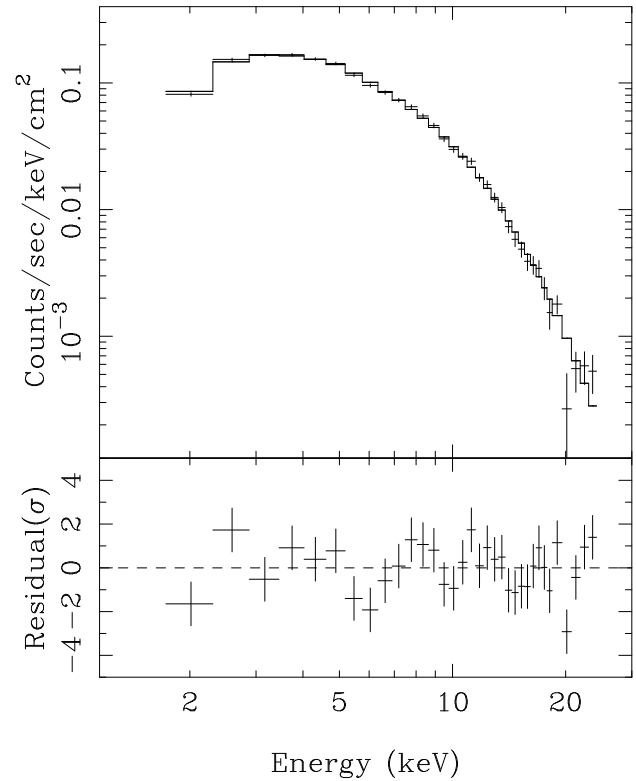


FIG. 8.—Example of the burst spectra and the fitting result by COMPST + BBODY corresponding to the time interval E shown in Fig. 6.

TABLE 6  
BEST-FIT PARAMETERS FOR REFLECTION MODEL (BURST)

DATA	DIRECT COMPONENT			REFLECTED COMPONENT			$\chi^2(\text{dof})$
	$F_b^a$	$kT_b^b$	$R_b^c$	$F_b$	$kT_b$	$R_b$	
C .....	$7.66^{+1.83}_{-1.66}$	$1.81^{+0.24}_{-0.22}$	$8.14^{+1.03}_{-1.43}$	$11.82^{+9.03}_{-15.14}$	$2.12^{+0.32}_{-0.91}$	$7.42^{+5.62}_{-8.02}$	1.76(30)
D .....	$3.88^{+0.63}_{-0.62}$	$1.43^{+0.15}_{-0.16}$	$9.30^{+1.29}_{-1.57}$	$9.33^{+5.17}_{-7.44}$	$1.89^{+0.25}_{-0.37}$	$8.26^{+4.31}_{-6.32}$	1.31(30)
E .....	$1.90^{+0.25}_{-0.22}$	$1.31^{+0.13}_{-0.13}$	$7.77^{+1.05}_{-1.31}$	$3.57^{+1.90}_{-3.20}$	$2.01^{+0.35}_{-0.53}$	$4.50^{+2.52}_{-4.48}$	1.42(30)
F .....	$0.94^{+0.17}_{-0.15}$	$1.18^{+0.18}_{-0.18}$	$6.78^{+1.49}_{-2.10}$	$1.81^{+1.18}_{-2.57}$	$2.14^{+0.58}_{-1.07}$	$2.85^{+2.06}_{-5.36}$	0.76(30)

NOTE.—Quoted errors are 90% confidence limits.

<sup>a</sup> Bolometric flux of blackbody in units of  $10^{-9}$  ergs  $\text{cm}^{-2}$   $\text{s}^{-1}$ .

<sup>b</sup> Blackbody temperature in units of keV.

<sup>c</sup> Blackbody radius in units of km.

TABLE 7  
COMBINED ANALYSIS OF THE BURST AND PERSISTENT EMISSION

DATA	COMPST		BBODY			
	$F_{\text{COMPST}}^a$	$\tau$	$F_b$	$kT_b^b$	$R_b^c$	$\chi^2(\text{dof})$
A .....	$10.12^{+1.68}_{-2.77}$	$13.38^{+2.63}_{-2.19}$	$8.74^{+3.00}_{-3.14}$	$2.32^{+0.24}_{-0.13}$	$5.31^{+0.58}_{-0.62}$	0.93(30)
B .....	$10.80^{+2.04}_{-0.41}$	$12.14^{+1.50}_{-1.26}$	$15.94^{+1.47}_{-1.81}$	$1.78^{+0.08}_{-0.08}$	$12.17^{+0.73}_{-0.88}$	0.44(30)
C .....	$14.12^{+2.78}_{-2.83}$	$16.49^{+1.76}_{-1.62}$	$7.32^{+1.30}_{-1.90}$	$1.86^{+0.19}_{-0.22}$	$7.53^{+1.05}_{-1.47}$	1.75(30)
D .....	$11.89^{+2.90}_{-8.64}$	$15.56^{+1.26}_{-1.50}$	$4.59^{+0.77}_{-0.78}$	$1.53^{+0.15}_{-0.21}$	$8.89^{+1.88}_{-2.30}$	1.15(30)
E .....	$10.87^{+1.62}_{-1.54}$	$14.91^{+0.68}_{-0.79}$	$2.65^{+0.40}_{-0.40}$	$1.41^{+0.13}_{-0.16}$	$7.93^{+1.57}_{-1.88}$	1.38(30)
F .....	$10.60^{+1.26}_{-1.14}$	$14.03^{+0.64}_{-0.62}$	$1.66^{+0.39}_{-0.47}$	$1.55^{+0.22}_{-0.28}$	$5.19^{+1.30}_{-1.89}$	0.63(30)

NOTE.—Quoted errors are 90% confidence limits. The electron temperature of COMPST is fixed as the value 3.31 keV, obtained from the spectra just before the burst.

<sup>a</sup> Flux of COMPST in units of  $10^{-9}$  ergs  $\text{cm}^{-2}$   $\text{s}^{-1}$ .

<sup>b</sup> Blackbody temperature in units of keV.

<sup>c</sup> Blackbody radius in units of km.

Planck function is fitted to the net burst emission, will give rise to systematic errors in the temperature, which affects the radius determination when the net burst flux is small compared to the persistent blackbody component. They show that near the end of a burst, the fitted blackbody temperatures become independent of the net burst flux, and the apparent blackbody radius artificially becomes very small. This effect was found to be important in a burst observed from the luminous source GX 17 + 2 (Sztajno et al. 1986), in which the blackbody component contributes  $\sim 40\%$  to the persistent emission. Thus, we made a spectral analysis of the combined (burst plus persistent) emission in terms of a two-component spectral model consisting of a variable blackbody BBODY and a fixed disk component COMPST, as done by Sztajno et al. (1986). However, this model could not explain the spectra, i.e., the spectral features in the net burst. The resulting reduced  $\chi^2$  are larger than 2.0 for 32 dof for spectra C and D, and 3.5 for 32 dof for spectrum E.

From an analysis of two bursts from the “dipping” source 1916–053, one of which occurred during a dip, Smale et al. (1992) found evidence that the bursts cause an approximately threefold increase in the emission component from the disk and an almost instantaneous ionization of the absorbing medium along the line of sight. Then, since there is a possibility that the above-mentioned hard excess is due to an increase of the disk component, we let the disk component in the model vary during the burst. Table 7 shows the result when the Comptonization model COMPST is adopted as the disk component. In some cases, the limited data do not allow us to make accurate determinations of all parameters, and thus we used the fixed electron temperature  $kT_e$ , calculated from the persistent emission data right before the burst. The  $\chi^2_\nu$  does not improve much, but the scattering depth  $\tau$  and the flux of the disk component increase during the burst for this particular model, as can be seen in the table. Figure 8 shows an example of burst spectrum E and the fitting result by COMPST + BBODY. A systematic wavy feature in the residuals seen in Figure 8, which cannot be described in terms of a spectral hardening alone, does not disappear regardless of the models we tried in the present analysis. It should be noted that van Paradijs et al. (1990) also found similar features in very energetic burst spectra from 2127+119 in M15.

## 5. DISCUSSION

### 5.1. Persistent Emission

During our observations the persistent X-ray flux (1–37 keV) of 1735–444 varied between  $7.3 \times 10^{-9}$  and  $11 \times 10^{-9}$  ergs  $\text{cm}^{-2}$   $\text{s}^{-1}$ , a higher level than previously observed. The source shows the characteristics of an atoll source in a high-intensity state. This confirms the conclusion of Hasinger & van der Klis (1989) that the differences between atoll sources and Z sources are caused by some additional basic aspect, rather than by a difference in the average mass accretion rate alone.

In the present analysis of simultaneous *Ginga* and *ROSAT* observation of 1735–444, the use of a Comptonization model plus a blackbody provides good fits. The blackbody component contributes  $\sim 15\%$ – $28\%$  of the total flux in this work. Smale et al. (1986) used only a power-law component with an exponential cutoff to fit *EXOSAT* data

of 1735–444 observed in 1985 August when the luminosity was low, while van Paradijs et al. (1988b) included the blackbody component in addition to the unsaturated Comptonization component to fit *EXOSAT* data observed in 1985 August when the luminosity was high. Hasinger & van der Klis (1989) have performed again the analysis of the *EXOSAT* data (see also Shultz, Hasinger, & Trümper 1989). They showed that 1735–444 occupied the island state when its luminosity was low, and the banana state when its luminosity was high. Thus it seems that the relative contribution of the blackbody component in 1735–444 depends on the luminosity. It is interesting to note that for 1705–440 (Langmeier et al. 1987) and 1957+115 (Singh, Apparao, & Kraft 1994) the blackbody component was detected only when the source intensity was high. Also, White, Stella, & Parmar (1988) extensively studied various types of two-component models and showed that the spectrum of the bright LMXBs can be well represented by the COMPST + BBODY model, while the spectra of faint sources can be understood in terms of a single COMPST component.

Many authors considered the correlation or anticorrelation between the spectral hardness and the intensity from the observation of LMXBs. White, Charles, & Thorstensen (1980) discovered “Sco X-1 type” behavior, i.e., a hardness-intensity correlation, from a series of *Copernicus* and *Ariel* observations of 1735–444. Ponman (1982) found from *Ariel* observation that 1735–444 shows a positive correlation between hardness and intensity at least some of the time and shows, in addition, a long-term, monotonic spectral softening. The present analysis of *Ginga* data also shows the positive correlation. However, *EXOSAT* observations of 1735–444 have shown both an anticorrelation between spectral hardness and intensity (Smale et al. 1986) and a positive hardness-intensity correlation (Penninx et al. 1989). Smale et al. (1986) understood the relation between hardness and intensity as a result of Compton cooling of a hot plasma. A similar model was used by Breedon et al. (1986) to explain the hardness-intensity anticorrelation observed from a burst source 1636–536.

Present observation may lead us to the following scenario regarding 1735–444. The blackbody radiation, which is believed to arise from the neutron star surface or the boundary layer between the neutron star surface and the inner accretion disk, may play an important role in the energy spectrum of the atoll sources when the sources are in the banana states. In this state, the luminosity is relatively high and the blackbody radiation may heat the ambient plasma in the disk (corona) enough to maintain its temperature at about a constant level in spite of the Compton cooling. Stronger blackbody radiation produces more ionizations, and, hence, the scattering depth  $\tau$  increases. This may explain the hardness-intensity correlation observed at high intensity. These features are consistent with our fitting results shown in Figure 5. On the other hand, when the accretion rate is low, the blackbody radiation is small and cannot heat the ambient plasma sufficiently, so that the fast cooling of these plasmas yields anticorrelation between the flux and the hardness, as discussed by Smale et al. (1986). Bildsten (1993, 1995) argued that the X-ray bursts and VLFN are fed from the same source (i.e., nuclear fuel) and that most fuel is consumed by X-ray bursts at the low accretion rate  $\dot{M}$  and by VLFN at the high  $\dot{M}$ . This suggests that the VLFN is closely related to the blackbody component

and supports the idea that the blackbody component contributes significantly to the spectral formation only in the banana state (i.e., at high  $\dot{M}$ ).

## 5.2. Burst

A strong burst with radius expansion from 1735–444 was reported previously by van Paradijs et al. (1988a), and Damen et al. (1990). Nevertheless, the burst we observed is unusual in that it occurred at a high persistent intensity,  $1.1 \times 10^{-8}$  ergs cm $^{-2}$  s $^{-1}$ , which is equivalent to the luminosity  $1.3 \times 10^{38}$  ergs s $^{-1}$  at an assumed distance 10 kpc, close to the Eddington luminosity  $L_{\text{Edd}}$ , and it still accompanied radius expansion (re). If we adopt a peak flux of  $F_{\text{re}} \sim 1.53 \times 10^{-8}$  ergs cm $^{-2}$  s $^{-1}$ , the ratio  $\gamma$  of persistent X-ray flux to peak burst flux is  $\sim 0.72$ , much higher than for a typical type I burst source. The high  $\gamma$ -value reflects the high persistent luminosity. The burst duration  $\tau$ , defined as the ratio of the burst fluence  $E_b$  to the peak burst flux  $F_{\text{re}}$ , is less than 6.3 s. Estimated  $\log \gamma$  and  $\log \tau$  values locate the 1735–444 in the lower right-hand corner of Figure 2 in van Paradijs et al. (1988a); they follow the  $(\gamma, \tau)$  correlation found for several other sources. The burst fluence  $E_b$  and the burst duration  $\tau$  of the burst observed in the present study, in the highest intensity state so far observed, are not much different from those observed previously (Lewin et al. 1980; van Paradijs et al. 1988b). The short duration of the burst indicates the absence of a significant contribution from hydrogen to the burst energy budget (Fujimoto, Hanawa, & Miyaji 1981). We cannot estimate the ratio,  $\alpha$ , of the average persistent flux to the time-averaged flux emitted in bursts because there were many interruptions of a few minutes to about 30 minutes due to Earth occultations and passage through the high particle background, and only one burst was observed. If we assume that no burst occurs during the interruptions of the observation, which might be true since 1735–444 was in a very high luminosity state, the lower limit of  $\alpha$  is estimated to be  $\sim 13,500$ .

Van Paradijs et al. (1979) pointed out that the high-luminosity sources generally do not burst, even though their observational properties are very similar to the X-ray bursters. In addition, there exists observational evidence from several burst sources that the burst activity is associated with the persistent luminosity level (Clark et al. 1977; Makishima et al. 1983; Gottwald et al. 1987; Lewin et al. 1987; see Lewin et al. 1993 for a recent review). In 1735–444, the highly irregular burst behavior and a ten-

dency for the bursts to come in clusters may be related to the fact that the persistent luminosity of this source is close to a critical value above which X-ray bursts do not occur, as expected from some thermonuclear flash models (Lewin et al. 1980; van Paradijs et al. 1988b; Fujimoto et al. 1981; Ayasli & Joss 1982). Kahn & Grindlay (1984) detected burstlike events from two bright Z-type sources, Cyg X-2 and GX 17+2. Tawara et al. (1984) and Sztajno et al. (1986) observed more X-ray bursts from GX 17+2, and Sztajno et al. (1986) concluded that these bursts are of type I. Recently, Kuulkers, van der Klis, & van Paradijs (1995) also found nine burstlike events in *EXOSAT* data of the Z source Cyg X-2. These observations are very similar to ours in that they observed bursts in a high-luminosity state, i.e., at a high  $\gamma$ -value. Thus, in high-luminosity burst sources, small perturbations appear to give rise to irregular burst behavior, which may depend on the thermal history of the neutron star.

Lewin et al. (1980) and van Paradijs et al. (1988b) argued from the apparent pattern of clustering of the bursts, visible in both the *SAS 3* and *EXOSAT* data, that the bursts themselves create conditions that are unfavorable for the recurrences of further bursts. Lapidus, Nobili, & Turolla (1994) divide the burst sources into three classes according to the mass accretion rate. They found that in all cases in which there is a high mass accretion rate, the adiabatic cooling time of the envelope,  $t_{\text{cool}}$ , is larger than the interburst time  $\Delta t$ . The source 1735–444 might belong to the group having the highest mass accretion rate, and thus with a cooling time of the envelope larger than the interburst time. The cluster of bursts could increase the temperature sufficiently to lift the degeneracy of the helium layer, giving rise to stable helium burning. The temperature of the helium layer could decrease after some time, and the layer could become sufficiently degenerate again for a cluster of bursts to occur.

The helium burning at high mass accretion rates may occasionally become locally unstable; this can result in weak X-ray bursts, and only patches on the neutron star may burn (Bildsten 1993, 1995). In this case, the blackbody radius during the bursts would be significantly smaller than the radius of a neutron star. However, the burst we observed at the high-intensity state accompanies radius expansion, which implies a strong burst consuming most of the accreted fuel and cannot be reconciled with the simple burning-patch model. Such strong bursts might be related to the thermal history of the neutron star from which the combustion speed is determined.

## REFERENCES

- Ayasli, S., & Joss, P. C. 1982, *ApJ*, 256, 637  
 Beskin, G. Neizvestny, S., Plokhhotnichenko, V., Popova, M., Zhuravkov, A., Benvenuto, O. G., Feinstein, C., & Méndez, M. 1994, *A&A*, 289, 141  
 Bildsten, L. 1993, *ApJ*, 418, L21  
 ———. 1995, *ApJ*, 438, 852  
 Breedon, L. M., Turner, M. J. L., King, A. R., & Courvoisier, T. J. L. 1986, *MNRAS*, 218, 487  
 Clark, G. W., Li, F. K., Canizares, C., Hayakawa, S., Jernigan, G., & Lewin, W. H. G. 1977, *MNRAS*, 179, 651  
 Corbet, R. H. D., et al. 1989, *MNRAS*, 239, 533  
 Corbet, R. H. D., Thorstensen, J. R., Charles, P. A., Menzies, J. W., Naylor, T., & Smale, A. P. 1986, *MNRAS*, 222, 15P  
 Damen, E., Magnier, E., Lewin, W. H. G., Tan, J., Penninx, W., & van Paradijs, J. 1990, *A&A*, 237, 103  
 Day, C. S. R., & Done, C. 1991, *MNRAS*, 253, 35P  
 Done, C., Mulchaey, J. S., Mushotzky, R. F., & Arnaud, K. A. 1992, *ApJ*, 395, 275  
 Ebisawa, K., Inoue, H., Mitsuda, K., Nagase, F., Tanaka, Y., Yaqoob, T., & Yoshida, K. 1992, in *Frontiers of X-Ray Astronomy*, ed. K. Koyama & H. Kunieda (Tokyo: University Academy Press), 301  
 Fujimoto, M. Y., Hanawa, T., & Miyaji, S. 1981, *ApJ*, 246, 267  
 Gottwald, M., Haberl, F., Parmar, A. N., & White, N. E. 1987, *ApJ*, 323, 575  
 Grindlay, J. E., McClintock, J. E., Canizares, C. R., van Paradijs, J., Cominsky, L., Li, F. K., & Lewin, W. H. G. 1978, *Nature*, 274, 10  
 Guilbert, P. W., & Rees, M. J. 1988, *MNRAS*, 238, 729  
 Haberl, F., Stella, L., White, N. E., Priedhorsky, W. C., & Gottwald, M. 1987, *ApJ*, 314, 266  
 Hasinger, G., & van der Klis, M. 1989, *A&A*, 225, 79  
 Hirano, T., Hayakawa, S., Nagase, F., Masai, K., & Mitsuda, K. 1987, *PASJ*, 39, 619  
 Imamura, J. N., Steiman-Cameron, T. Y., & Middleditch, J. 1987, *ApJ*, 320, L41  
 Kahn, S. M., & Grindlay, J. E. 1984, *ApJ*, 281, 826  
 Kuulkers, E., van der Klis, M., & van Paradijs, J. 1995, *ApJ*, 450, 748  
 Langmeier, A., Sztajno, M., Hasinger, G., Trümper, J., & Gottwald, M. 1987, 323, 288  
 Lapidus, I., Nobili, L., & Turolla, R. 1994, *ApJ*, 433, 287  
 Lewin, W. H. G., Hoffman, J. A., Doty, J., Li, F. K., & McClintock, J. E. 1977, *IAU Circ.* 3075

- Lewin, W. H. G., Penninx, W., van Paradijs, J., Damen, E., Sztajno, M., Trümper, J., & van der Klis, M. 1987, *ApJ*, 319, 893
- Lewin, W. H. G., van Paradijs, J., Cominsky, L., & Holzner, S. 1980, *MNRAS*, 193, 15
- Lewin, W. H. G., van Paradijs, J., & Taam, R. E. 1993, *Space Sci. Rev.*, 62, 223
- Lightman, A. P., & White, T. R. 1988, *ApJ*, 335, 57
- Makino, F., & The ASTRO-C Team. 1987, *Astrophys. Lett. Commun.*, 25, 223
- Makishima, K., et al. 1983, *ApJ*, 267, 310
- McClintock, J. E., Canizares, C. R., Bradt, H. V., Doxsey, R. E., Jernigan, J. G., & Hiltner, W. A. 1977, *Nature*, 270, 320
- Mitsuda, K. 1992, in *Frontiers of X-Ray Astronomy*, ed. K. Koyama & H. Kunieda (Tokyo: University Academy Press), 115
- Mitsuda, K., et al. 1984, *PASJ*, 36, 741
- Nakamura, N., Dotani, T., Inoue, H., Mitsuda, K., Tanaka, Y., & Matsuoka, M. 1989, *PASJ*, 41, 617
- Penninx, W., Hasinger, G., Lewin, W. H. G., van Paradijs, J., & van der Klis, M. 1989, *MNRAS*, 238, 851
- Pfeffermann, E., et al. 1987, *Proc. SPIE*, 733, 519
- Ponman, T. 1982, *MNRAS*, 201, 769
- Serlemitsos, P. J., & Swank, J. H. 1980, preprint
- Shultz, N. S., Hasinger, G., & Trümper, J. 1989, *A&A*, 225, 48
- Singh, K. P., Apparao, K. M. V., & Kraft, R. P. 1994, *ApJ*, 421, 753
- Smale, A. P., Corbet, R. H. D., Charles, P. A., Menzies, J. W., & Mack, P. 1986, *MNRAS*, 223, 207
- Smale, A. P., Mukai, K., Williams, O. R., Jones, M. H., & Corbet, R. H. D. 1992, *ApJ*, 400, 330
- Sunyaev, R. A., & Titarchuk, L. 1980, *A&A*, 86, 121
- Sztajno, M., van Paradijs, J., Lewin, W. H. G., Langmeier, A., Trümper, J., & Pietsch, W. 1986, *MNRAS*, 222, 499
- Tawara, Y., Hirano, T., Kii, T., Matsuoka, M., & Murakami, T. 1984, *PASJ*, 36, 861
- Trümper, J. 1983, *Adv. Space Res.*, 2(4), 241
- Turner, M. J. L., et al. 1989, *PASJ*, 41, 345
- van Amerongen, S., Pedersen, H., & van Paradijs, J. 1987, *A&A*, 185, 147
- van Paradijs, J., Dotani, T., Tanaka, Y., & Tsuru, T. 1990, *PASJ*, 42, 633
- van Paradijs, J., Joss, P. C., Cominsky, L., & Lewin, W. H. G. 1979, *Nature*, 280, 375
- van Paradijs, J., & Lewin, W. H. G. 1985, *A&A*, 157, L10
- van Paradijs, J., & McClintock, J. E. 1995, in *X-Ray Binaries*, ed. W. H. G. Lewin, J. van Paradijs, & E. P. J. van den Heuvel (Cambridge: Cambridge Univ. Press), 58
- van Paradijs, J., Penninx, W., & Lewin, W. H. G. 1988a, *MNRAS*, 233, 437
- van Paradijs, J., Penninx, W., Lewin, W. H. G., Sztajno, M., & Trümper, J. 1988b, *A&A*, 192, 147
- Vrtilek, S. D., McClintock, J. E., Seward, F. D., Kahn, S. M., & Wargelin, B. J. 1991, *ApJS*, 76, 1127
- White, N. E., Charles, P. A., & Thorstensen, J. R. 1980, *MNRAS*, 193, 731
- White, N. E., Peacock, A., Hasinger, G., Mason, K. O., Manzo, G., Taylor, B. G., & Branduardi-Raymont, G. 1986, *MNRAS*, 218, 129
- White, N. E., Peacock, A., & Taylor, B. G. 1985, *ApJ*, 296, 475
- White, N. E., Stella, L., & Parmar, A. N. 1988, *ApJ*, 324, 363
- Yoshida, K., Mitsuda, K., Ebisawa, K., Ueda, Y., Fujimoto, R., Yaqoob, T., & Done, C. 1993, *PASJ*, 45, 605